NUMERICAL INVESTIGATION ON THE CAGE-TO-CAGE WAKE EFFECT: A CASE STUDY OF A 4x2 CAGE ARRAY

Jaesub Sim
Department of Mechanical and Structural Engineering and Materials science,
University of Stavanger,
4036, Stavanger, Norway
Email: j.sim@stud.uis.no

Hui Cheng
Department of Mechanical and Structural Engineering and Materials science,
University of Stavanger,
4036, Stavanger, Norway
Email: hui.cheng@uis.no

Karl Gunnar Aarsæther
Department of Technology and Safety,
UiT The Arctic University of Norway,
9037 Tromsø, Norway
Email: karl.g.aarsather@uit.no

Lin Li
Department of Mechanical and Structural Engineering and Materials science,
University of Stavanger,
4036, Stavanger, Norway
Email: lin.li@uis.no

Muk Chen Ong
Department of Mechanical and Structural Engineering and Materials science,
University of Stavanger,
4036, Stavanger, Norway
Email: muk.c.ong@uis.no

Abstract

Aquaculture has been the world's fastest-growing food producing method and grown to become the second-largest export industry in Norway during the past 40 years. Usually, the high-value fish such as Atlantic Salmon (*Salmo Salar*) is raised in a multi-cage fish farm, where the flow interactions between fish cages exist. In this study, the interactions between fish cages are implemented into the numerical program, FhSim, to investigate its influences on the responses of a multi-cage fish farm. Tensions in anchor lines, drag force and cultivation volume of each cage in a full-scale 4x2 multi-cage fish farm under different flow directions are analysed numerically. The discrepancies of the responses based on three cases, *i.e.*, (*i*) without any wake effects, (*ii*) with only cage-to-cage wake effect and (*iii*) with all the wake effects, are compared and discussed. The results indicate that neglecting the wake effects will overestimate the total drag force of the eight cages up to 128% and underestimate the total cultivation volume of the eight cages as much as 42%. This study can provide suggestions on how to consider the wake effects during the design of the multiple-cage system.

1 Introduction

Demands for seafood from a growing population has coincided with a decline in the product supplied from wild-caught fish. Marine aquaculture has the potential to increase food production from coastal regions in order to meet the need for seafood. A typical marine fish farm consists of 4 ~ 12 fish cages, and these fish cages are arranged in a regular grid [1]. Mooring loads are an important consideration when designing marine fish farms, and the forces from interaction with the incoming flow velocity for each fish cage combine to make the total mooring load. An individual fish cage might experience different flow velocities depending on the direction of the global current and the wakes downstream of the other fish cages in the mooring grid. The flow field in a marine aquaculture site should be accurately predicted, in order to fulfil the precision fish farming [2], especially in terms of mechanical load and water exchange.

Theoretical and numerical studies have been conducted to investigate the flow characteristics behind nets and fish cage. Løland [3] proposed an empirical expression for the velocity reduction behind a net panel based on model testing (r=1-0.46C_D, r is the velocity reduction factor, C_D is the drag coefficient of a net panel) and applied this expression to represent the wake effect after a fish cage. The empirical expression gives a uniform reduced flow throughout the entire wake. However, the flow field after a circular net structure is not uniform since the flow is not always perpendicular to the net panel due to different locations of the twines and the deformation of the fish cage. Endresen *et al*. [4] developed a numerical model for the wake effect using Morison-type force model associated with the flow velocity based on Blevins formula [5]. Bi and Xu [6] numerically simulated the flow field around a 4x2 fish farm using the porous-media model. However, the deformation of the fish cage was not considered in the simulations. Zhao et al. [7, 8] applied the porous-media model to study the flow reduction behind a net panel.

A few experiments were conducted to investigate the wake effect among fish cages in an array. Bi et al. [9] conducted experiments to investigation the reduction in flow velocity

downstream from a net panel. Turner *et al.* [10] conducted an experiment in a large flume tank to measure the drag forces of each square cages within a 2x3 array. The results showed that when the cages were aligned in a flow direction, the drag forces on the second and the third cages are reduced approximately 50% and 75%, respectively, compared to that of the first cage. Gansel *et al.* [11] conducted experiments to measure the wake characteristics behind a circular fish cage by using Particle Image Velocimetry (PIV) method. The results indicated that the flow velocity was reduced up to 40% behind the fish cage and increased 20% at the flanks of the fish cage. Zhao et al. [12] conducted a series experiments to study the tension force in mooring lines under different configuration of fish cages. The results indicated that the 4 × 2 configurion is optimal from a perspective of construction cost.

Based on these previous work [6, 10, 11], the wake behind a fish cage should be treated as nonuniform. However, the non-uniform wake profile has not been implemented into any finite element (FE) solver today. In the present research, the flow characteristics behind the permeable net cages are implemented into a FE solver, FhSim, to simulate a 4×2 multi-cage fish farm under pure current conditions. To investigate how the wake effect behind a fish cage affect the structural responses of a multi-cage fish farm, three cases, *i.e.*, (*i*) without any wake effects, (*ii*) with only cage-to-cage wake effect, (*iii*) with all the wake effects (twine-to-twine wake effect, net-to-net wake effect and cage-to-cage wake effect), are applied in the present study. The drag force and cultivation volume of each fish cage, and tensions in all anchor lines are calculated and used to discuss the influence of wake effects.

2 Description of the Multiple-cage system

A typical Norwegian salmon fish farm consists of 4~12 circular fish cages. As shown in Cardia and Lovatelli [1], the fish cage is between 20 to 50 meters deep, 50 meters in diameter, and holds up to 200, 000 salmon. In the present study, a typical Norwegian fish cage is chosen for the numerical analysis. The fish cage includes a double-pipe floating

collar, a cage net (cylindrical net structure with conical bottom), cables (connecting cage net and sinker tube), a sinker tube and a centre point weight. A schematic description of a single fish cage is shown in Fig. 1, and a list of relevant parameters and dimensions of the numerical model are given in Table 1.

Figure 2 shows the plan view of a multiple-cage system with a 4x2 configuration which is applied in the present study. The red and green arrows on the Cage 1 represent the global coordinate system as the X and Y axes. The Z-axis is pointing into the paper. The eight cages are numbered in order from 1 to 8 along the positive X-axis. The anchor lines are denoted with U1-U6 and V1-V10. The flow directions of 0° and 90° are expressed as blue arrows on the upper left corner of Fig. 2.

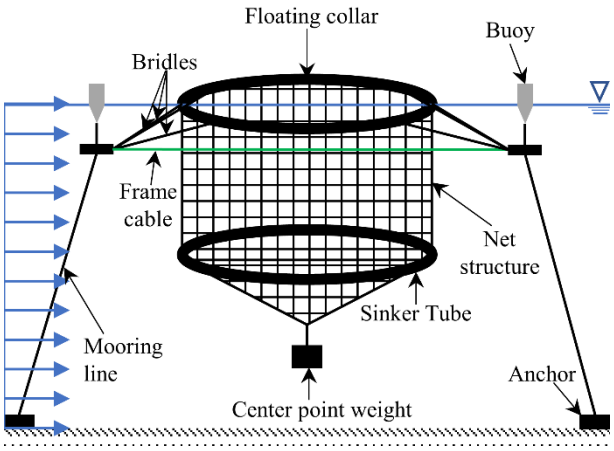

Figure 1. Overview of a single gravity-based fish cage.

Table 1: Dimensions and properties of the fish cage in the present study.

Sub model	Parameter	Value	Unit
Floating Collar	Inside diameter	51	m
	Outside diameter	53	m
	Section diameter	0.25	m
	Wall thickness	28.4	mm
	Young's modulus	0.9	GPa
	Linear density	81	kg/m
Net structure	Twine diameter	2.5	mm
	Mesh length	25	mm
	Solidity	0.2	-
	Twine density	1125	kg/m^3
	Twine Young's modulus	0.1	GPa
	Vertical cylinder depth	15	m
	Conical bottom depth	28	m
Sinker Tube	Tube diameter	51	m
	Section diameter	0.25	m
	Center point weight	100	kg
	Linear density	51	kg/m
Buoy	Diameter	2	m
	Vertical cylinder depth	1	m
	Conical bottom depth	2	m

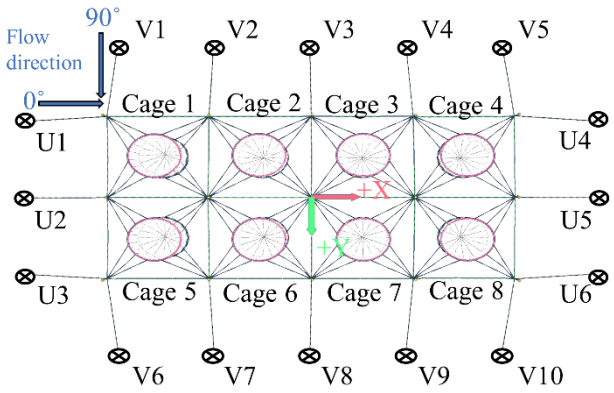

Figure 2. Configuration of 4x2 multi-cage fish farm layout.

3 Numerical methods

3.1 FhSim Framework

FhSim is a numerical program developed by SINTEF Ocean, which is capable of performing dynamic responses of fish cages under different environmental conditions. Model creation, interconnection, and initialization are based on the modular sections in the input file [13]. The structural responses of fish cages are acquired by solving Ordinary Differential Equations (ODEs) in the time domain [14]. The dynamic responses of gravity-based fish cages obtained using FhSim have been validated extensively against experiments. The validations showed satisfactory results, particularly for low flow velocities, where the deviations of drag force between the numerical and experimental results are as low as 7% [13,14].

3.2 Hydrodynamic force model

Net structures are discretized with the triangular elements using the method developed by Priour [15], and the triangular elements are connected through nodes at the corners. Hydrodynamic forces of individual twines are computed using the Morison-type force

model and distributed among the nodes on the corresponding triangular element [15]. The individual twines are regarded as smooth cylinders. In this study, the hydrodynamic forces acting on the net element is calculated by summing each force on individual twine within the net element using Morison's equation [4]. In case of inclined twines due to the geometry or deformation of the cage, the velocity components which are normal and tangential to the twine should be taken into account in order to compute the drag forces with crossflow principle (Eq. 1).

$$F_N = 0.5 C_N \rho A |U_N| U_N$$
$$F_T = 0.5 C_T \rho A |U_T| U_T \qquad \text{Eq. 1}$$

Where, U_N and U_T are the normal and tangential components of the ambient flow velocity, respectively. C_N, C_T are the normal and tangential drag coefficients, which are dependent on Reynolds number (*Re*). A is the reference area which is the product of the length and the diameter of a twine. C_T is assigned with an unchangeable value of 0.01 for all the *Re*, C_N is taken from the experimental data as a seventh order polynomial function of the logarithmic *Re* which is limited in the range of $10^{1.5}$ and 10^4 (Eq. 2) [16].

$$\begin{aligned} C_N = {} & -78.46675 + 254.73873(log_{10}Re) - 327.8864(log_{10}Re)^2 \\ & + 223.64577(log_{10}Re)^3 - 87.92234(log_{10}Re)^4 \\ & + 20.00769(log_{10}Re)^5 - 2.44894(log_{10}Re)^6 \\ & + 0.12479(log_{10}Re)^7 \end{aligned} \qquad \text{Eq. 2}$$

where $Re = \frac{U_{net} d_t}{\nu}$, $U_{net} = \frac{\sqrt{2-S_n}}{\sqrt{2(1-S_n)}} U_\infty$, d_t is the diameter of a twine, ν is the kinematic viscosity of water, S_n is solidity ratio, and U_∞ is the incident flow velocity.

3.3 Wake effects

Wake effects are essential and complex in analyses of permeable structures, such as the nets in fish cage and fishing gear, since wake effects can alter the incoming flow velocity at a downstream structure by the presence of upstream structures. As the hydrodynamic force acting on the twine is proportional to the square of the flow velocity, it is imperative to discern the variation of the flow velocity to get precise force prediction. The wake region in a multi-cage system is decomposed into two domains for ease of implementation (see Fig. 3). One is within a cage, and the other is outside of a cage. The former comprises two wake effects, twine-to-twine wake effect and net-to-net wake effect, and the latter is the cage-to-cage wake effect [17].

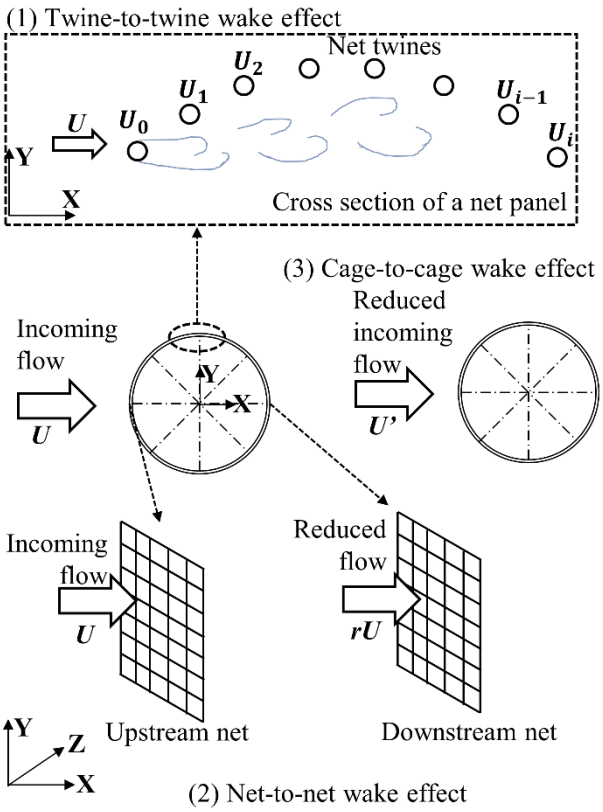

Figure 3. Illustration of different wake effects [17]. *(*1) Twine-to-twine wake effect, where a grid of *i+1* cylinder (cross-section of a net panel) are exposed to an incident flow velocity $\boldsymbol{U}$. The $\boldsymbol{U_i}$ (i = 0, 1 …) denotes the velocity experienced by cylinder i, which is modified due to the presence of upstream cylinders. (2) net-to-net wake effect, where the upstream (left) net panel is exposed to an incoming flow velocity $\boldsymbol{U}$. The net-to-net wake effects from the upstream net panel result in a reduced flow ($\boldsymbol{rU}$) at the downstream net panel. (3) Cage-to-cage wake effect, where the incoming flow for the downstream (right) fish cage is nonuniform and might be smaller than the incoming flow for the upstream (left) fish cage.

3.3.1 Twine-to-twine wake effect

Twine-to-twine wake effect represents the interaction between the twines in a net panel. This effect has an influence region in the order of centimetres (see Fig. 3). Endresen *et al.*

[4] proposed a method to account this wake effect by replicating the velocity profile for the downstream twines. The replicated velocity profile is adapted from Blevins virtual origin formula (Eq. 3) [5].

$$r_{twine} = 1.02\sqrt{\frac{C_d}{6 + x/d}}\,exp\left\{\frac{-(y/d)^2}{0.0767C_d(6 + x/d)}\right\} \quad \text{Eq. 3}$$

where r_{twine} is the normalized velocity defect downstream from a twine placed at the origin (X=0, Y=0), d is the diameter of the twine, and C_d is the drag coefficient for a circular cylinder as a function of Reynolds number [5]. The positive X-axis is oriented along the direction of flow.

3.3.2 Net-to-net wake effect

The net-to-net wake effect represents the interaction between net panels in a single fish cage. This effect has an influence region in the order of tens of meters (see Fig. 3). Approximately, half of the net panels in a cylindrical fish cage are in the wake region of the upstream net panels. The velocity reduction factor, $r = 1 - 0.46C_D$, is introduced to FhSim to represent the net-to-net wake effect, where C_D is the drag coefficient of a net panel when the flow is perpendicular to the net panel [3]. The velocity reduction factor is regarded as forming a uniform shape of wake [18].

$$U_{downstream} = rU_{upstream} \quad \text{Eq. 4}$$

In simulations, whether a panel in the wake can be determined based on its central position, the centre of the fish cage and the incoming flow direction (see Fig. 4). Then, the flow

reduction factor can be set as an attribute of the downstream net panels to reduce its incident velocity.

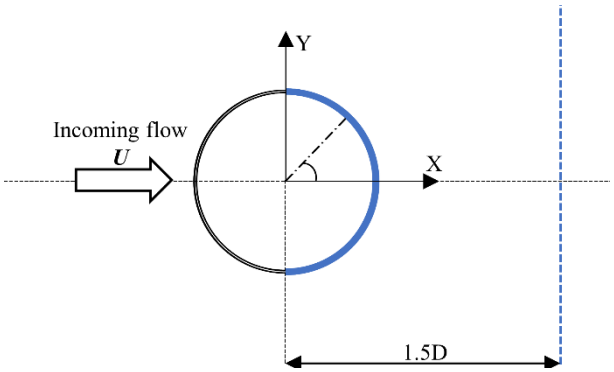

Figure 4. A plane view of a fish cage for illustrating of the method to identify the nets which experience the net-to-net wake effect.

3.3.3 Cage-to-cage wake effect

The cage-to-cage wake effect represents the interaction between fish cages. This effect has an influence region in the order of a few hundred meters (see Fig. 3). In marine aquaculture, fish cages are usually grouped in arrays as a fish farm. The flow experienced by the downstream cages is affected by the existence of the upstream cage mainly because of two effects. One is the blockage of the flow which makes the water go around the cage, and the other is the wake formed by the inflow through the net cage since recirculation and backflows occur in the region [4]. In the present study, the change in velocity is replicated by a curve fitting according to the experiment by Gansel *et al.* [11]. Fig. 5 shows the flow defect factor along a horizontal line (the blue dash line in Fig. 4) at $1.5D$ behind a fish cage which is symmetrical about $Y/D = 0$. With the increasing distance to the axis of symmetry, the flow defect factor first decreases, and then becomes steady. When the distance to the axis of symmetry is approximately $0.65D$, the velocity reaches the undisturbed velocity (the same as incoming flow velocity). When the distance to the axis of symmetry exceeds $0.65D$, the flow velocity is slightly higher than the incoming velocity due to the conservation of mass. The blue curve in Fig. 5 is a Fourier series as given in Eq. 5.

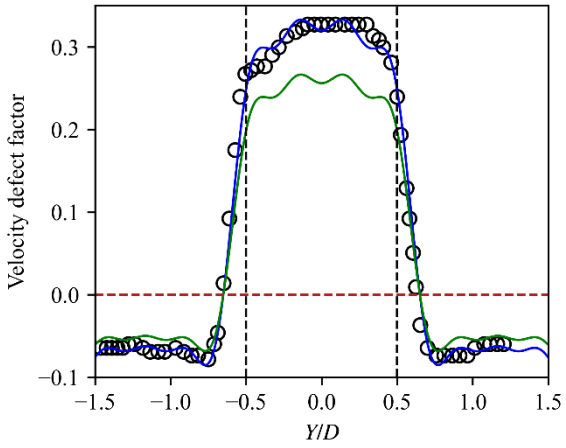

Figure 5. Velocity profile 1.5D downstream behind a fish cage according to the experiment done by Gansel et al. [11]. Black circles represent the experimental data with a solidity ratio of 0.25, the blue line is the curve fitting to the data, and the green line is the scaled velocity profile for a solidity ratio of 0.2. Y is the axis perpendicular to the flow direction, D is the diameter of the fish cage.

$$\begin{aligned} V_r = {} & 0.1201 + 0.2414cos(\omega y/D) + 0.0115cos(2\omega y/D) \\ & - 0.0644cos(3\omega y/D) + 0.0030cos(4\omega y/D) \\ & + 0.0294cos(5\omega y/D) - 0.0058cos(6\omega y/D) \\ & - 0.0149cos(7\omega y/D) \end{aligned} \qquad \text{Eq. 5}$$

Where $\omega = 2.692$. In the present study, the width of the wake region behind a cage is implemented as 2D thus, $-1 < y/D < 1$. The velocity profile in Eq. 5 is then extended to different solidity ratios and distances behind an upstream fish cage as Eq. 6.

$$V_{decay} = V_r \cdot \frac{S_n}{0.25}\sqrt{exp\left(-\frac{x/D - 1.5}{25}\right)} \quad \text{Eq. 6}$$

Where *Vr* represents the velocity defect factor when *Sn* = 0.25, *Sn* is the solidity ratio of the net. In addition, the reduced velocity factor decays as it propagates downstream, x/D is the nondimensionalized distance after the upstream fish cage in the flow direction. V_{decay} represents the velocity defect factor at different coordinates after a fish cage and is used in the present study. The incoming flow for the downstream cage, ***U'***, is calculated by Eq. 7, where ***U*** is the incoming flow for the upstream cage.

$$\boldsymbol{U'} = (1\text{-}V_{decay})\boldsymbol{U} \quad \text{Eq. 7}$$

3.4 Structural model

Cables, ropes and other components with cable-like properties are modelled by bar elements [19]. The sinker tube is modelled by a version of the generic cable model in which the two endpoints are connected to create a continuous cable structure. The buoy is modelled as vertical circular cylinders with a conical bottom. It is given 5 DOF where rotation around its vertical axis is omitted. The floating collar is modelled as a flexible continuous circular ring. It is divided into sections, and for each section, the radial and vertical responses are calculated by the Euler beam equations (Eq. 8).

$$F_R(s,t) = m\frac{\partial^2 v}{\partial t^2} + EI\left(\frac{\partial^4 v}{\partial s^4} + \frac{1}{R^2}\frac{\partial^2 v}{\partial s}\right) \quad \text{Eq. 8}$$

$$F_Z(s,t) = m\frac{\partial^2 z}{dt^2} + EI\frac{\partial^4 z}{ds^4}$$

where v and z are the radial and vertical responses of the floater respectively, m is the per unit length mass of the floater, EI is the bending stiffness of the floater, F_R is the per unit length radial force on the floater and F_Z is the per unit length vertical force on the floater.

The net structure is calculated based on a well-established method, in which net panels of arbitrary shape are described by dividing the original shape into triangular net elements [15]. Structural forces acting within the structure are computed separately for each net panel and then distributed between the nodes associated with the panel element. It can be referred to [14] for more details on the net structure model in FhSim.

FhSim supports the use of several different integration methods, including Euler methods, Heun's method and Runge-Kutta methods, and facilitates a suitable framework for implementing additional methods [14]. In this study, it employs Runge-Kutta method with variable time steps to solve the motion equation.

3.5 Volume estimation method

The volume of a cage is computed utilizing the tetrahedron volume integration method. As shown in Fig. 6, the cage is considered as a cylindrical cake which has *M* layers and *N* slices from top to bottom, and a piece is extracted and divided into three tetrahedrons [20]. Three vectors, $\vec{A}$, $\vec{B}$, and $\vec{C}$ are assigned along the sides of the tetrahedron by choosing one point as an origin. The volume of the small piece of cake can be computed using the principle of the scalar triple product (Eq. 9). Subsequently, the volume of a cage is obtained by summing up all the volume of tetrahedrons. In the present study, each fish cage is decomposed into 10 layers and 32 slices, and thus, 960 tetrahedrons.

$$V_{cage} = \frac{1}{6}\left\|\vec{A}\cdot\left(\vec{B}\times\vec{C}\right)\right\| = \frac{1}{6}\left[\left(a_1(b_2c_3 - c_2b_3) + a_2(b_3c_1 - c_3b_1) + a_3(b_1c_2 - c_1b_2)\right]\right. \quad \text{Eq. 9}$$

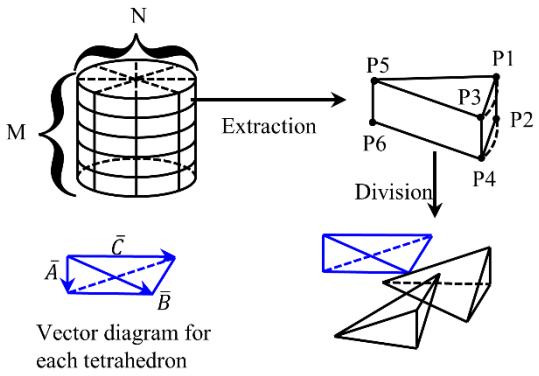

Figure 6. Tetrahedron volume integration method [21].

4 Results and discussion

4.1 Environmental loading

In the present study, only current is considered in the numerical analysis. Ten flow directions (from 0˚ to 90˚ with 10˚interval) are applied with a flow velocity of 0.5 m/s to investigate how the wake effects affect the structural responses of a multi-cage fish farm. The influence of the wake effects on (1) drag forces and cultivation volumes of individual fish cages, (2) total drag forces and cultivation volumes of the eight cages, (3) tensions in the anchor lines are compared and discussed based on the simulation matrix listed in Table 2. For each flow direction, a time-domain simulation of 500 seconds is performed, and the structural responses after the simulation reach equilibrium are used for discussions. Fig. 7 gives the time history for the estimated volume of Cage 1. It shows that the volume of a fish cage converges to a stable value approximately after 300 seconds, and thus, 500 seconds are long enough for simulations to reach equilibrium.

Table 2: Simulation matrix.

	Wake effect selection	Flow direction	Flow velocity
Case 1	without wake effects	0˚ to 90˚	0.5 m/s
Case 2	with only cage-to-cage wake effect	0˚ to 90˚	0.5 m/s
Case 3	with all the three wake effects	0˚ to 90˚	0.5 m/s

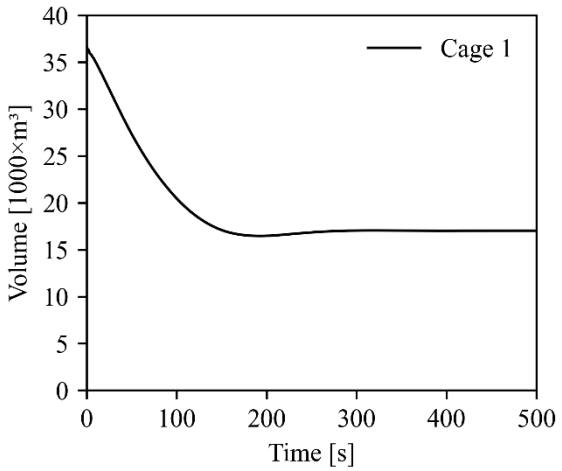

Figure 7. Time history for the estimated cage volume of Cage 1 with an incoming flow velocity of 0.5 m/s and 0° flow direction.

4.2 Wake effects on drag forces and cultivation volumes of fish cages under different flow directions

4.2.1 Case 1 (without wake effect)

Without wake effects, the blockage and alteration of flow field after the permeable net structure are neglected. All the fish cages are exposed to the same flow conditions, and thus, every triangular element on fish cages experiences the same flow velocity. Therefore, as shown in Figs. 8 and 9, the drag force and the cultivation volume of the eight fish cages are equal. In addition, due to the cylindrical shape of the fish cage, the drag force and cultivation volume become constant regardless of the change of the flow direction.

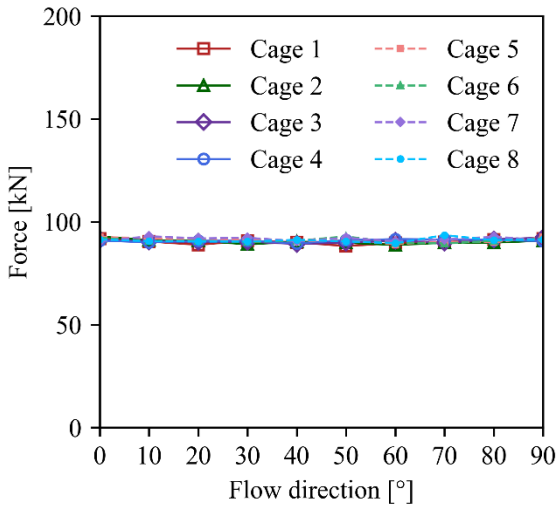

Figure 8. Drag force of the individual fish cages without wake effects (Case 1).

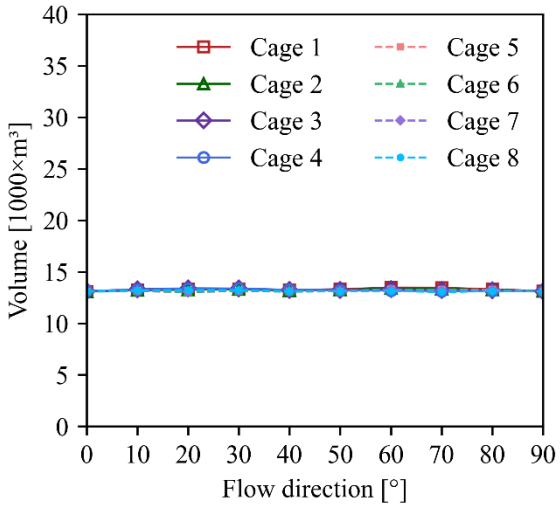

Figure 9. Cultivation Volume of the individual fish cages without wake effects (Case 1).

4.2.2 Case 2 (with only cage-to-cage wake effect)

In Case 2, the alteration of the flow field is realized by implementing the cage-to-cage wake effect according to Section 3.3.3. The two internal wake effects are not considered. As shown in Fig. 10, with the changing flow direction, the drag force of Cage 1 is unchangeable and keeps the same value as that in Case 1. The reason is that in both Case

1 and Case 2, no matter under which flow direction, Cage 1 always experiences the same flow velocity without any disturbance from the other cages. Except for Cage 1, the flow velocities experienced by other fish cages vary with the changing flow direction and different from that under the corresponding condition in Case 1. Therefore, fish cages at different positions experience different ambient flow velocities, and thus, drag force and cultivation volume of the individual cages can differ from each other.

As shown in Figs. 10 and 11, the drag force and cultivation volume of an individual fish cages are highly correlated, as larger cultivation volume comes with lower drag force. This relation is also seen in previous research [3, 9, 13, 16].

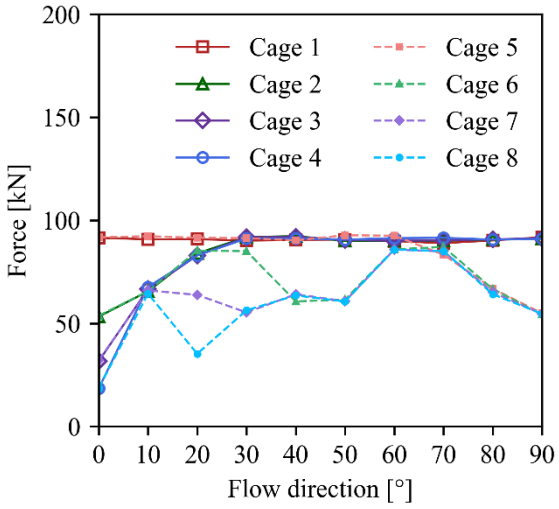

Figure 10. Drag force of the individual fish cages with only cage-to-cage wake effect (Case 2).

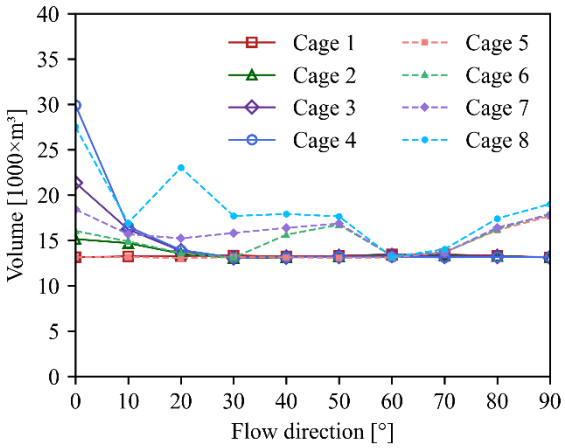

Figure 11. Cultivation Volume of the individual fish cages with only cage-to-cage wake effect (Case 2).

When the flow direction is 0°, the drag forces of the cages which are symmetric about the X-axis have the same value, *e.g.*, Cage 1 and Cage 5 have the same drag force when the flow direction is 0°. Because the flow comes along the X+ direction and the grid-like multi-cage fish farm is also symmetric about the X-axis, the cages which are symmetric about the X-axis experience the same flow velocity. Due to the existence of a cage-to-cage wake effect, the downstream fish cages experience a reduced flow velocity. Thus, the drag forces on Cage 2, 3 and 4 are reduced by 39%, 62%, and 76%, respectively.

With the increasing flow direction, the influences of cage-to-cage wake effect on Cage 2, 3 and 4 are reduced. As described in Section 3.3.3 and Eq. 5, the width of the wake region after a cage is twice the diameter of a fish cage in the present numerical model. Hence, the influence of the upstream cages on the flow field around the downstream cages (e.g. the influence of Cage 1 onto Cage 2) vanishes once the flow direction exceeds 48.6˚ as illustrated in Fig. 12. However, the width of the velocity decreasing zone within the wake region after a permeable net structure is found as approximately 1.3D as the flow velocity reaches the undisturbed flow velocity at ±0.65D (see Fig. 5). Thus, one can say that the reduction in flow velocity at a cage due to the presence of upstream cages diminishes once the flow direction exceeds a threshold angle, 35.1˚. This agrees well with the responses

(drag force and cultivation volume) of cage 2, 3, and 4 observed from Figs. 10 and 11, where the responses reach a similar value with Cage 1 after 30˚. Since Cage 2, 3, and 4 shall not experience the flow velocity reduction induced by the upstream cages once the flow direction is greater than 35.1˚, and thus, they show similar behavior as Cage 1. However, with the increasing flow direction, the influences of cage-to-cage wake effect on Cage 6, 7 and 8 are slightly complicated compared to Cage 2, 3 and 4. Because they might get influence from Cage 1, 2, 3 and 4, the drag force of Cage 6, 7 and 8 are smaller than Cage 1 in general.

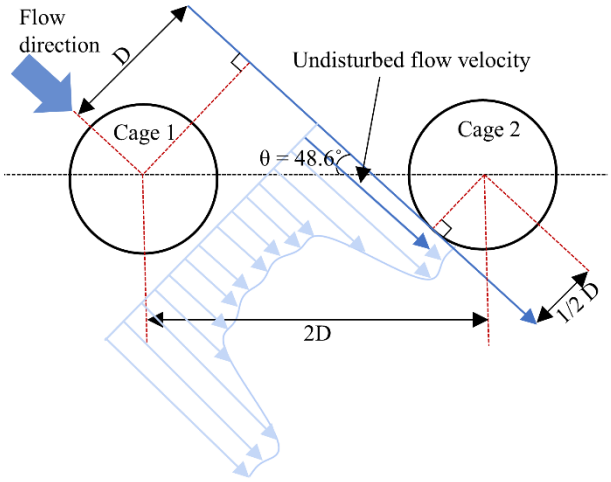

Figure 12. Flow interference of upstream cage to downstream cage. *D* is the diameter of a cage, and the θ is the flow direction. The illustration of the velocity profile with blue arrows is the velocity profile at 1.5D downstream from a cage.

Interestingly, when the flow direction is between 60°-70°, all cages have similar drag forces and cultivation volumes. That can be explained with Fig. 13, where the variation of the flow field induced by the wake region is presented. The blue area behind cages represents the velocity decreasing zone, and the red area at the flanks of the wake region represents the velocity increasing zone. The downstream cages 5, 6, 7, and 8 have both blue and red colors on them, which means parts of the twines on these cages experience a reduced flow velocity and parts of them experience an increased flow velocity. Thus, if the

effect of velocity increase compensates the effect of velocity decrease, the structural responses of the downstream fish cages should be similar to that of the upstream fish cages.

When the flow direction exceeds 70°, the downstream Cage 5, 6, 7 and 8 start to sit in the wake regions of Cage 1, 2, 3 and 4, respectively. When the flow direction is 90°, the four downstream fish cages are totally in the velocity decreasing zone, and thus, the drag force is reduced to a small value. As expected, that small value is the same with the drag force of Cage 2 when the flow direction is 0°.

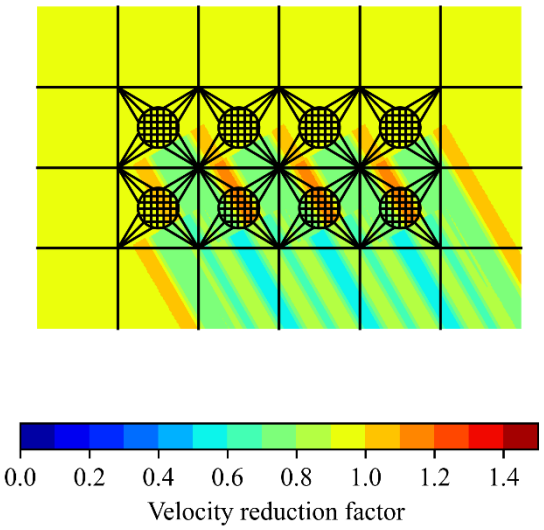

Figure 13. Illustration of the flow field around the fish farm when the flow direction is 60°. The color bar under the figure represents the velocity reduction factor according to the ambient flow velocity. Red color shows an increase of flow velocity, and the blue color shows a decrease in flow velocity.

4.2.3 Case 3 (with all the three wake effects)

In Case 3, all the three aforementioned wake effects are included in the numerical simulations. The two wake effects, *i.e.*, twine-to-twine wake effect and net-to-net wake effect, can reduce the flow velocity for the downstream twines and net panels inside a

single fish cage. Therefore, the drag force of each cage is decreased, and the cultivation volume of each cage is increased compared to that under the corresponding condition in Case 2. The changes of the drag force and the cultivation volume of individual cages with changing flow direction follow a similar trend as those with Case 2. These can be observed in Figs. 14 and 15.

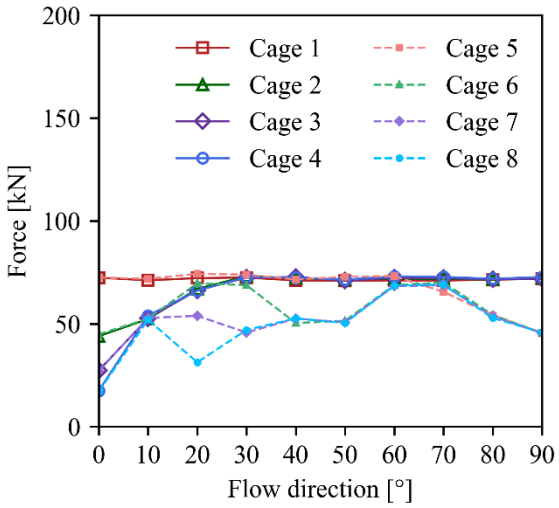

Figure 14. Drag force of the individual fish cages with all the three wake effects (Case 3).

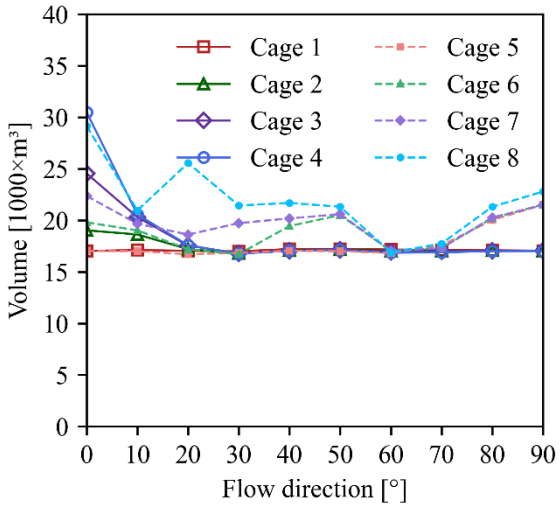

Figure 15. Cultivation volumes of the individual fish cages with all the three wake effects (Case 3).

4.2.4 Comparison between the three cases

Among all the cages, Cage 8 experiences the most significant variations in both drag force and cultivation volume. To have a better comparison between the three cases, the responses of the downstream cage, Cage 8, are discussed in Section 3.2.4.

The differences in the cultivation volume of Cage 8 based on the three cases are shown in Fig. 16. As explained in Section 4.2.1, the cultivation volume of Cage 8 based on Case 1 is constant with the flow directions. Compared to Case 3, Case 2 is always smaller, and the discrepancy between the two cases is almost constant with the flow directions. As mentioned in Section 4.2.3, that discrepancy comes from the two wake effects. As shown in Fig. 16, the discrepancy at 0° is slightly smaller than the other flow directions. The reason for that might come from the twine-to-twine wake effect. The twine-to-twine wake effect varies with the angle between flow direction and the normal vector of the triangular element. As the cage deforms by the current loads, the twine-to-twine wake effects are altered due to the change of this angle. The smaller the cage deforms, the less the twine-to-twine wake effect contributes. When the flow direction is 0°, the small deformation of

Cage 8 moderates the influence of the twine-to-twine wake effect on it, and thus, the discrepancy of the cultivation volume between Case 2 and Case 3 is small.

As shown in Figs. 16 and 17, Cage 8 experiences a sudden change in drag force and cultivation volume when the flow direction is 20˚ for both Case 2 and Case 3. That can be explained with Fig. 18, where the red and blue areas illustrate the flow velocity increase and reduction due to cage-to-cage wake effect. As shown in Fig. 18, the blue on Cage 8 is the darkest among the eight cages, which means the ambient flow velocity for Cage 8 is the smallest. Therefore, it is reasonable that Cage 8 experiences the smallest drag force and largest cultivation volume among all cages, when the flow direction is 20° as the velocity decreasing zones are superimposed the most on Cage 8.

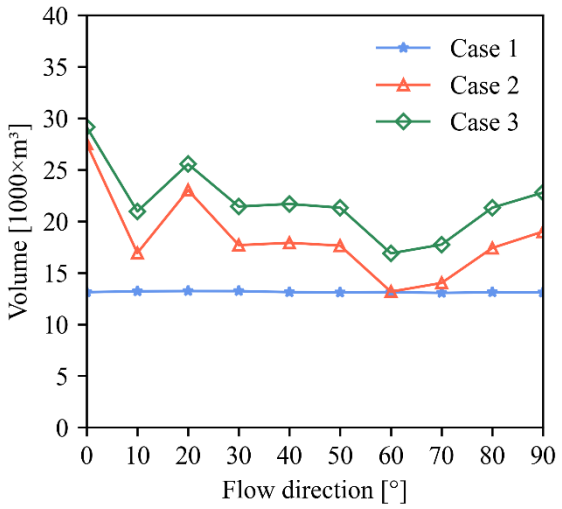

Figure 16. Comparison of the cultivation volume of Cage 8 in different cases.

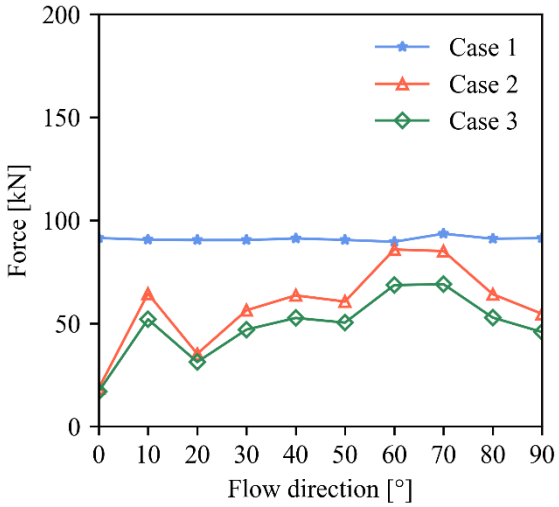

Figure 17. Comparison of the drag force of Cage 8 in different cases.

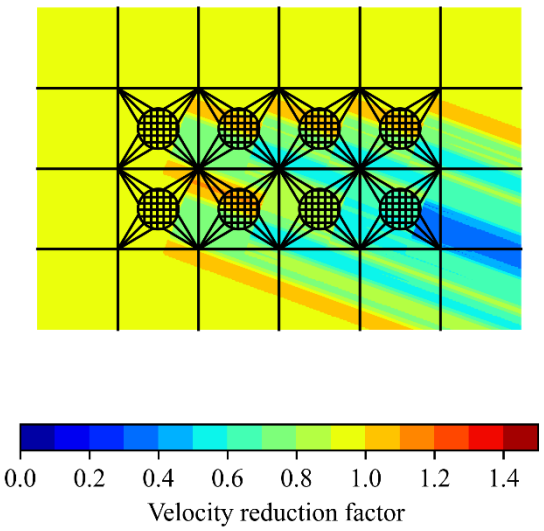

Figure 18. Illustration of the flow field around the fish farm when the flow direction is 20°. The colour bar under the figure represents the velocity reduction factor according to the ambient flow velocity. Red colour shows an increase of flow velocity, and the blue colour shows a decrease in flow velocity.

4.3 Wake effects on the total drag force and cultivation volume under different flow directions

The total cultivation volume and drag force of all the eight fish cages are presented in Figs. 19 and 20, respectively, to show how the wake effects influence structural responses with different flow directions. The total cultivation volume of the eight fish cages is highly correlated with the total drag forces. The larger volume corresponds to a lower drag force. Thus, the change of the drag force with respect to the flow direction follows the opposite trend as that for the cultivation volume.

As shown in Figs. 19 and 20, the total cultivation volume and drag force in Case 1 are constant with the flow directions. Because no wake effect is applied in Case 1, each fish cage has the same flow condition for different flow directions, and thus, the sum of the drag force of each fish cage is constant with the flow directions. With the same reason, the sum of the cultivation volume of each cage is constant with the flow directions as well.

The change of the total drag force with different flow directions in Case 2 and 3 have the same trend. The total drag force first increases with the increasing flow direction when the flow direction is less than 30°, then keeps similar value when the flow direction is between 30°-50°, next increases to the highest value when the flow direction is 60°, and finally decreases when the flow direction exceeds 70°. The trend of the total cultivation volume follows the opposite trend as that of the total drag force. This trend of changes in total drag force and cultivation volume with different flow directions can be explained by the cage-to-cage wake effect. With the changing flow direction, the flow velocities experienced by fish cages vary, and thus, the total drag force and cultivation volume are changed. However, compared to Case 3, the total drag force of Case 2 is averagely 20% smaller, and the total cultivation volume is averagely 25% larger. These discrepancies between the two cases are almost constant with different flow directions. As explained in Section 4.2.4, these discrepancies come from the two internal wake effects, *i.e.*, twine-to-twine wake effect and net-to-net wake effect, and agree with the previous research regarding the wake effects on drag force of a single fish cage [6] .

Interestingly, when the flow direction is 60°, the total drag force of the eight cages in Case 2 is similar to that in Case 1. As explained in Section 4.2.2, all cages in Case 2 have similar structural responses due to the flow direction and the mooring configuration.

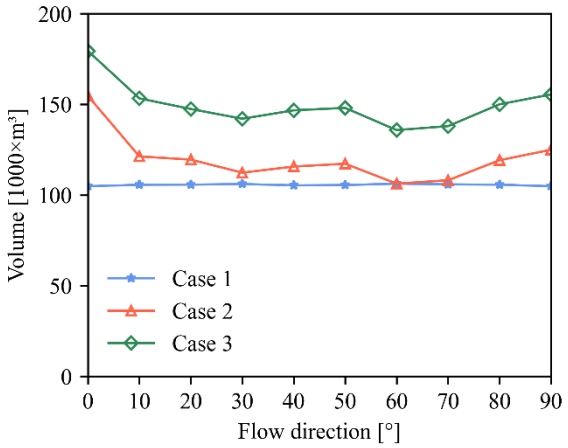

Figure 19. Comparison of the total cultivation volume of all cages in different cases.

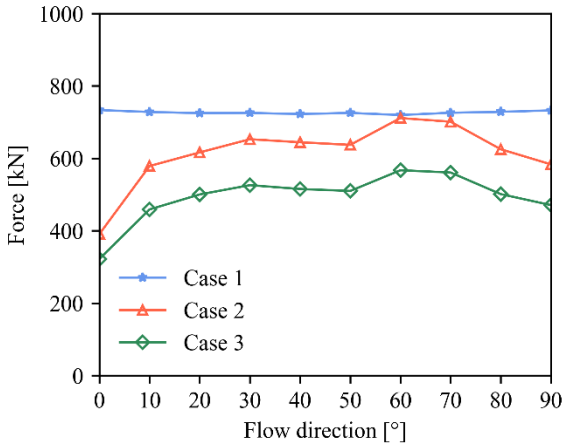

Figure 20. Comparison of the total drag force of all cages in different cases.

4.4 The wake effects on tensions in anchor lines under different flow directions

The extreme tension in anchor lines (ETAL) is defined as the maximum tension in all the 16 anchor lines under a given flow direction. The sum of the environmental loads is

distributed to the anchors according to the mooring system configuration and flow directions. As shown in Fig. 21, the maximum ETAL among all the flow directions based on Case 1, 2, and 3 are 274.5 kN, 241.3 kN, and 204.5 kN, respectively.

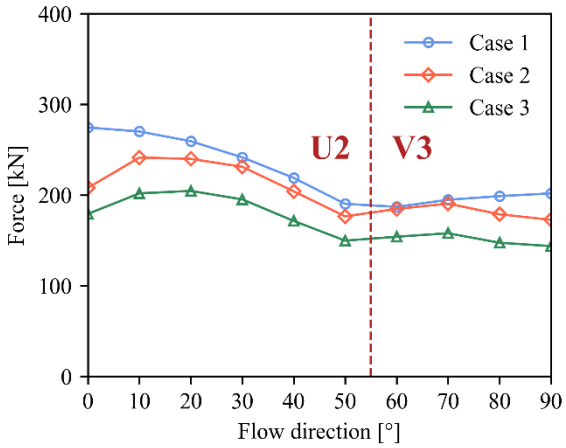

Figure 21. Comparison of ETAL based on the three cases when the ambient flow velocity is 0.5 m/s. The ETAL occurs in U2 when the flow direction < 50° and in V3 when the flow direction > 50°.

For Case 1, the ETAL first decreases, and then increases slightly with the increasing flow direction. As expected, the ETAL and total drag force change differently with flow directions. As shown in Fig. 20, the total drag force in Case 1 is constant with flow directions, which means the same amount of current load is distributed to the anchor lines. Because the number of anchor lines that contribute to holding the current load varies as the flow direction changes, ETAL changes with flow directions. Therefore, the change of ETAL with different flow directions in Case 1 only comes from the different tension distributions among the anchor lines.

For Case 2 and 3, the change of ETAL with different flow directions has the same trend. With the increasing flow direction, ETAL increases at the beginning then reduces until 50˚ and keeps a similar value. Different from Case 1, the change of ETAL with flow directions

in Case 2 and 3 come from both the total drag force of the eight cages and the force distribution among anchor lines. When the drag forces from the fish cages transfer to the mooring system, the forces are distributed according to the flow direction and the mooring configuration. Thus, the changes of ETAL with different flow directions in Case 2 and 3 are determined by the total drag force and the configuration of the mooring system.

5 Conclusion

The objective of this study is to identify the influence of the wake effects on the structural responses of a 4x2 multi-cage fish farm. From the performed numerical simulations, the impacts of wake effects on drag forces, cultivation volumes, and tensions in anchor lines are clearly seen. The following are the main results from this study:

1) With all the three wake effects, the drag force on a single cage reduces by 39%, 62% and 76%, as the flow passes through one, two, and three cages, respectively, when the flow direction is 0° and velocity is 0.5 m/s.
2) With all the three wake effects, the cultivation volume of a single cage increases by 12%, 44% and 79% as the flow passes through one, two, and three cages respectively, when the flow direction is 0˚ and velocity is 0.5 m/s.
3) Without the two internal wake effects*, i.e.,* twine-to-twine wake effect and net-to-net wake effect, the drag force of a single fish cage is overestimated by 19%, and the cultivation volume of a fish cage can be underestimated by 26%.
4) The flow direction and the flow field disturbed by the presence of fish cages can influence the maximum tension in anchor lines. Regardless of flow directions, the maximum tension in anchor lines with all wake effects is reduced up to 35% compared to that without wake effects.

References

[1] Cardia, F. and Lovatelli, A., 2015. Aquaculture operations in floating HDPE cages: a field handbook. FAO Fisheries and Aquaculture Technical Paper, (593).

[2] Føre, M., Frank, K., Norton, T., Svendsen, E., Alfredsen, J.A., Dempster, T., Eguiraun, H., Watson, W., Stahl, A., Sunde, L.M. and Schellewald, C., 2018. "Precision fish farming: A new framework to improve production in aquaculture". biosystems engineering, 173, pp.176-193.

[3] Løland, G., 1991. "Current forces on and flow through fish farms", PhD thesis, NTNU, Trondheim, Norway.

[4] Endresen, P. C., Føre, M., Fredheim, A., Kristiansen, D., Enerhaug, B., 2013. "Numerical modeling of wake effect on aquaculture nets", Proceedings of the ASME 2013 32nd International Conference on Ocean, Offshore and Arctic Engineering – OMAE.

[5] Blevins, R. D., 2001. Flow-Induced Vibration, Krieger Publishing Company, Malabar, United States.

[6] Bi, C. W., Xu, T. J., 2018. "Numerical study on the flow field around a fish farm in tidal current", Turkish Journal of Fisheries and Aquatic Sciences, Vol. 18, 705-716.

[7] Zhao, Y.-P., Bi, C.-W., Dong, G.-H., Gui, F.-K., Cui, Y., Guan, C.-T., Xu, T.-J., 2013. Numerical simulation of the flow around fishing plane nets using the porous media model. Ocean Engineering 62, 25–37.

[8] Zhao, Y.-P., Bi, C.-W., Dong, G.-H., Gui, F.-K., Cui, Y., Xu, T.-J., 2013. Numerical simulation of the flow field inside and around gravity cages. Aquacultural Engineering 52, 1–13.

[9] Bi, C.-W., Zhao, Y.-P., Dong, G.-H., Xu, T.-J., Gui, F.-K., 2013. Experimental investigation of the reduction in flow velocity downstream from a fishing net. Aquacultural Engineering 57, 71–81.

[10] Turner, A. A., Jeans, T. L., Reid, G. K., 2016. "Experimental investigation of fish farm hydrodynamics on 1:15 scale model square aquaculture cages", Journal of Offshore Mechanics and Arctic Engineering, Vol. 138(6), 061201.

[11] Gansel, L. C., McClimans, T. A., Myrhaug, D., 2008. "The effects of fish cages on ambient currents", Proceedings of the ASME 27th International Conference on Offshore Mechanics and Arctic Engineering.

[12] Zhao, Y.-P., Bi, C.-W., Chen, C.-P., Li, Y.-C., Dong, G.-H., 2015. Experimental study on flow velocity and mooring loads for multiple net cages in steady current. Aquacultural Engineering 67, 24–31.

[13] Reite, K. J., Føre, M., Aarsæther, K. G., Jensen, J., Rundtop, P., Kyllingstad, L., Endresen, P. C., Kristiansen, D., Johansen, V., Fredheim, A., 2014. "Fhsim - time domain simulation of marine systems", Proceedings of the International Conference on Offshore Mechanics and Arctic Engineering - OMAE, vol. 8.

[14] Endresen, P. C., Birkevold, J., Føre, M., Fredheim, A. Kristiansen, D., lader, P., 2014. "Simulation and validation of a numerical model of a full aquaculture net-cage system", Proceedings of the ASME international conference on Ocean, Offshore and Arctic Engineering – OMAE.

[15] Priour, D., 1999. “Calculation of net shapes by the finite element method with triangular elements”, Communications in numerical methods in engineering, vol. 15, 775-763.

[16] Cheng, H., Aarsæther, K. G., Li, L., and Ong, M. C., 2020. "Numerical Study of a Single-Point Mooring Gravity Fish Cage with Different Deformation-Suppression Methods", Journal of Offshore Mechanics and Arctic Engineering, Vol. 142(4): 041301.

[17] Cheng, H., Li, L., Aarsæther, K.G. and Ong, M.C., 2020. “Typical hydrodynamic models for aquaculture nets: a comparative study under pure current conditions”. Aquacultural Engineering, Vol. 90: p.102070.

[18] Kristiansen, T., Faltinsen, O. M., 2012. “Modelling of current loads on aquaculture net cages”, Journal of Fluids and Structures, Vol. 34, 218-235.

[19] Fredriksson, D. W., Decew, J., Lader, P., Volent, Z., Jensen, and Willumsen, F. V., 2014. “A finite element modeling technique for an aquaculture net with laboratory measurement comparisons”. Ocean Engineering, 83, pp. 99–110

[20] Huang, C. C., Tang, H. J., Liu, J. Y., 2006. “Dynamical analysis of net cage structures for marine aquaculture: Numerical simulation and model testing”, Aquacultural Engineering.

[21] Xu, Z. and Qin, H., 2020. Fluid-structure interactions of cage based aquaculture: From structures to organisms. Ocean Engineering, 217, p.107961.